Supporting Information

Sulfur-Anchored Azulene as Cathode Material for Li-S Battery

Zhenying Chen,†[a] Jörn Droste,†[b] Guangqun Zhai,[c] Jinhui Zhu,[a] Jun Yang,[a] Michael Ryan Hansen,*[b] Xiaodong Zhuang *[ac]

[a] The Soft2D Lab, State Key Laboratory of Metal Matrix Composites & Shanghai Key Laboratory of Electrical Insulation and Thermal Ageing, School of Chemistry and Chemical Engineering, Shanghai Jiao Tong University, Dongchuan Road 800, Shanghai 200240, China. E-mail: zhuang@sjtu.edu.cn

[b] Institute for Physical Chemistry, Westfälische Wilhelms-Universität Münster, Corrensstraße 28/30, 48149 Münster, Germany. E-mail: mhansen@uni-muenster.de

[c] Jiangsu Key Laboratory of Environmentally Friendly Polymeric Materials, School of Materials Science and Engineering, Changzhou University, Changzhou 213164, China.

Experimental section

Materials:

Azulene was synthesized according to reported literature.[1] Sublimed sulfur powder (99.98%) and ammonium peroxydisulfate ($(NH_4)_2S_2O_8$, AR) were purchased from Sigma-Aldrich, Hydrochloride solution (HCl, 32 wt%) and alcohol (AR) were purchased from Sinopharm Chemical Reagent Co., Ltd. Carbon disulfide (CS_2, AR) was purchased from TCI. All chemicals were used as received. The distilled water used was collected from a HHitech laboratory water purification system with a resistivity higher than 18.2 MΩ·cm.

Preparation of Az-S.

In a general procedure, sublimed sulphur powder (1.35 g, 5.27 mmol) without further purification and azulene (0.15 g, 1.17 mmol) were added to a long-stem funnel after manual grinding. And the vial was heated to 185 °C to form a homogeneous mixture under stirred for 6 h. The black solid was taken directly from the vial after cooling to room temperature. All the reactions were performed under nitrogen atmosphere.

Preparation of polyazulene (PAz).

The polymerization method is the same as the method for polymerization of aniline. Specifically, azulene (2 g, 15.6 mmol) was dissolved in 1.0 M HCl (200 mL) in an Erlenmeyer flask. Ammonium peroxydisulfate (4.45 g, 19.5 mmol) in 50 ml water was then added dropwise under ambient condition. After stirring at room temperature for 24 h, black powder was collected by vacuum filtration. The crude product was washed by distilled water and alcohol three times, respectively, and then dried in vacuum at 60 °C for 12 h.

Materials characterization.

The morphology and structure of the samples were recorded using a scanning electron microscope (Nova NanoSEM 450, FEI company, USA) and transmission electron microscope (JEM-2100, JEOL Ltd., Japan) respectively. XRD was conducted with a X-ray diffractometer (D8 Advance, Bruker Corp., Germany) using Cu-Ka radiation (Cu K= 0.154056 nm). Thermogravimetric analysis (TGA) was performed with thermogravimetric analyzer (Discovery TGA550, TA, USA), where the temperature rose from 50° C to 800°C in argon with a heating rate of 20 K min^{-1}. The thermal characterization was carried out in the DSC (Q2000, TA instruments) from -40 °C to 140 °C with a heating rate of 20 K/min. X-ray photo electron spectroscopy (XPS) was measured at a X-ray photoelectron spectrometer (AXIS ULTRA DLD, Kratos Analytical Ltd., UK) with monochromatic Al Ka source (1486.6 eV). The electrodes for ex-situ XPS were prepared in an Argon atmosphere in a glove box and washed with DME three times before placed in a specific transfer device. Detailed characters of various chemical bonds were measured by a Raman microscope (DXR, Thermo Fisher Scientific Inc., USA) with a laser wavelength of 532 nm under ambient conditions and Fourier-transform infrared spectroscopy was measured (Spectrum 100, Perkin Elmer) by preparing KBr pellets. The sulfur content is determined by elemental analysis (Vario EL Cube).

Solid-state NMR

The $^{13}C\{^1H\}$ solid-state NMR measurements were carried out on a Bruker Avance III 300 spectrometer (B_0 = 7.05 T) using a 4.0 mm magic-angle spinning (MAS) WVT H/X double resonance probe. The samples were packed in a 4 mm o.d. ZrO_2 sealed with a Vespel© or a Kel-F© top cap. The magic angle was adjusted on $NaNO_3$ before each measurement if required. Adamantane was used as external reference for determining the radio-frequency field strength (ν_{RF}) and to calibrate the isotropic chemical shift scale for ^1H (δ =1.78 ppm with respect to TMS) and ^{13}C (δ

=29.5 ppm and 38.5 ppm with respect to TMS). All solid-state NMR spectra were recorded using a MAS frequency of 10.0 kHz and employed ν_{RF} = 62.5 kHz ($\tau_{90°}$ = 4.0 µs) and ν_{RF} = 50 kHz ($\tau_{90°}$ = 5.0 µs) for ^{1}H and ^{13}C, respectively. During the acquisition of ^{13}C heteronuclear decoupling of ^{1}H was achieved using the sw_f-TPPM sequence. For the $^{13}C\{^{1}H\}$ cross-polarization MAS (CP/MAS) experiments a 70 to 100 % ramp was used on the ^{13}C channel. The dipolar dephasing sequence of Mao and Schmidt-Rohr[2] was used for spectral editing with a dephasing time of 67 µs. The $^{13}C\{^{1}H\}$ CP/MAS NMR spectra of azulene and Az-S were recorded with a recycle delay of 60 s. The $^{13}C\{^{1}H\}$ CP/MAS NMR spectra of PAz and PAz-S were recorded with a recycle delay of 5 s. The quantitative direct polarization (DP) $^{13}C\{^{1}H\}$ MAS NMR spectra of PAz and PAz-S were recorded with recycle delays of 300 s and 150 s, respectively. Data analysis and plotting was done by using the Bruker Topspin 4.0.5 software and Python 3.7.0.

Molecular modeling and DFT calculations:

The DFT calculations were performed using TURBOMOLE[3,4] (version 6.5). The geometry optimization of all molecular structures employed the TPSS[5] functional and the def2-TZVP[6] basis set. The subsequent NMR chemical shift calculations were done with the def2-TZVP basis and the B3LYP[7,8] functional. Plotting of the calculated chemical shifts as Gaussian peaks was performed with Python 3.7.0.

Electrochemical measurements

Working electrodes were made using 70 wt% Az-S, 20 wt% super-P and 10 wt% sodium alginate as binder. the slurry was cast to aluminum foil and dried at 60 °C under vacuum for 12 h before used. The sulfur loading is about 0.8-1.0 mg cm^{-1}. CR2016 coin cells were assembled with lithium foil in an argon-filled glove box. The electrolyte was 1 M lithium bis-(trifluoromethanesulfonyl) imide (LiTFSI) and 2 wt% lithium nitrate ($LiNO_3$) in 1,3-dioxolane (DOL) and 1,2-dimethoxyethane (DME) (volume ratio 1:1), The batteries rest for 10 h before discharging and charging galvanostatically using a LAND-CT2001C battery test system within 1.8−2.8V. Cyclic voltammetry (CV) and electrochemical impedance spectroscopy (EIS) in the frequency range from 100 kHz to 10 mHz were conducted on EC-Lab electrochemical workstation.

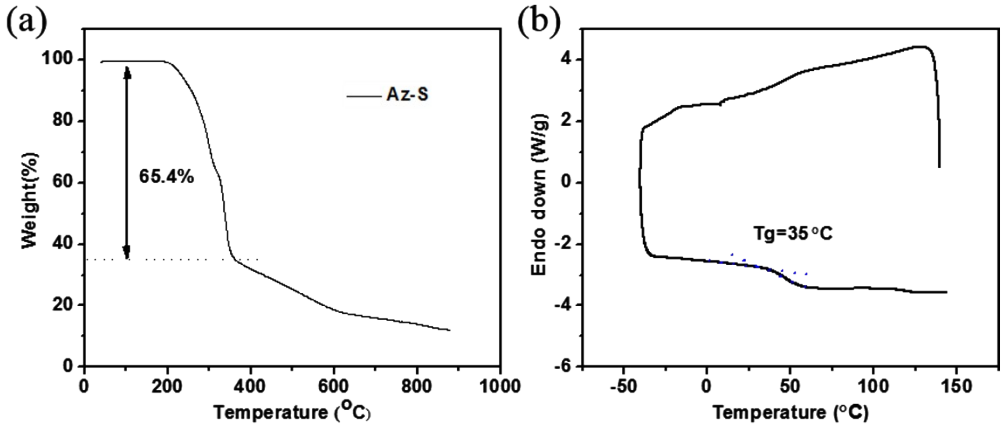

Fig. S1 (a) TGA of Az-S; (b) DSC curve of Az-S.

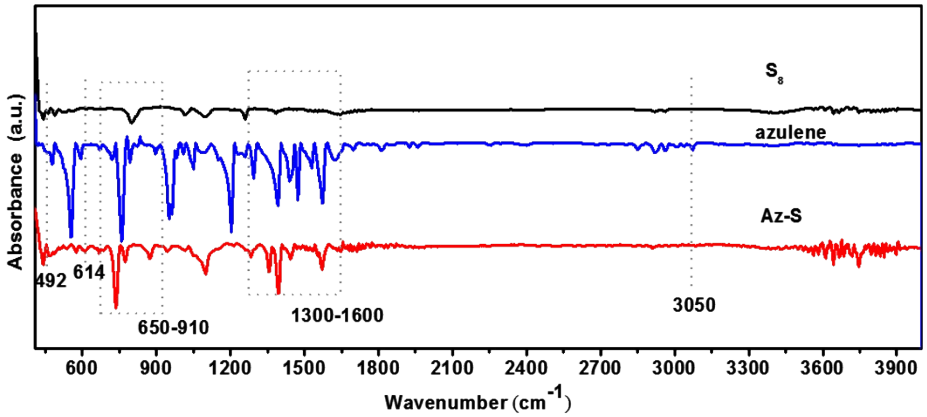

Fig. S2 FTIR spectra of S_8 (upper trace, black), azulene (lower trace, blue) and Az-S (lower trace, red).

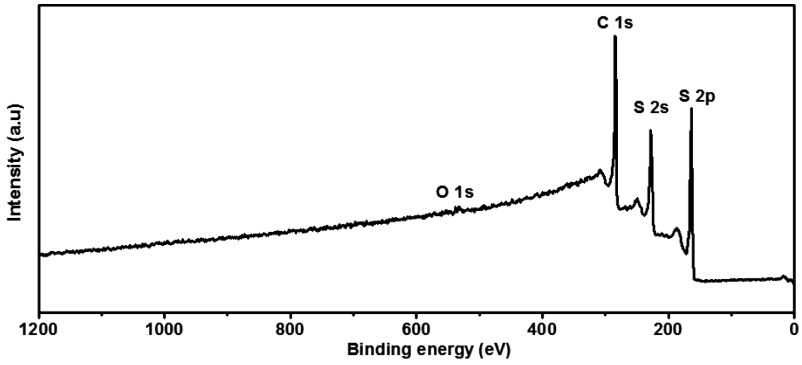

Fig. S3 XPS survey spectrum for Az-S.

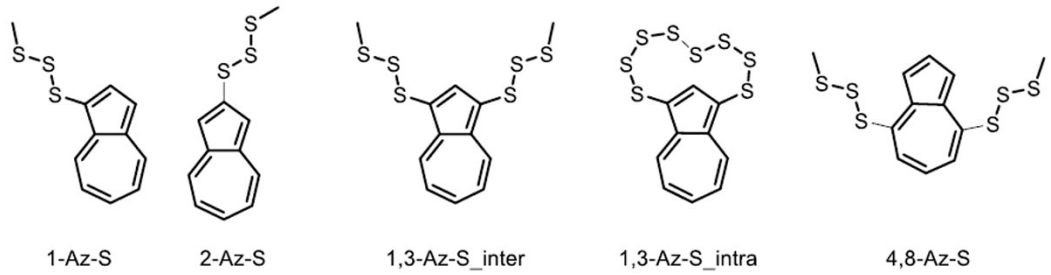

Fig. S4 Chemical structures of Az-S employed to investigate the influence of different sulfur-substitution patterns on the ^{13}C chemical shift.

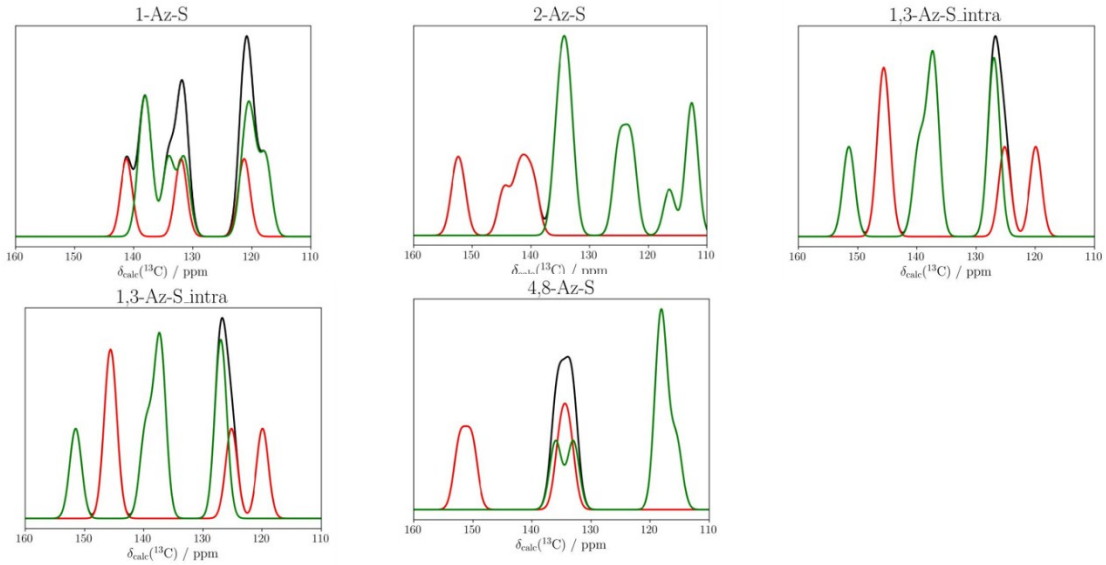

Fig. S5 Plots of the ^{13}C chemical shifts values resulting from DFT calculations of different sulfur-substitution patterns in Figure S4. Color code: C_q + CH_x (black), C_q (red), CH_x (blue). All calculated ^{13}C shifts are plotted assuming a Gaussian linewidth of 75 Hz.

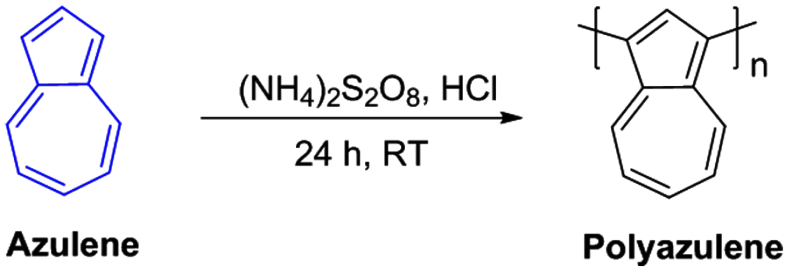

Fig. S6 Synthesis scheme of polyazulene.

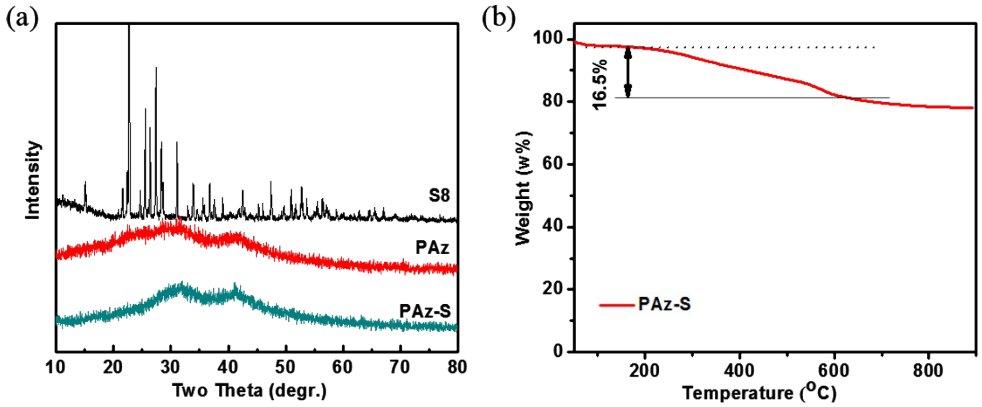

Fig. S7 (a) X-ray diffraction patterns of sulfur (S_8), PAz, and PAz-S. (b) TGA curve of PAz-S under N_2 atmosphere.

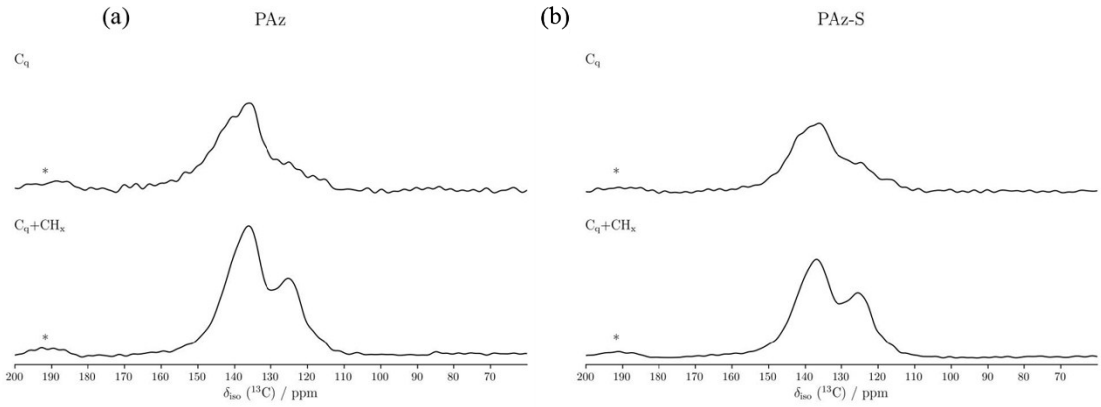

Fig. S8 $^{13}C\{^1H\}$ CP/MAS NMR spectra recorded at 7.05 T employing a MAS frequency of 10.0 kHz and a CP time of 1.0 ms for (a) PAz and (b) PAz-S.

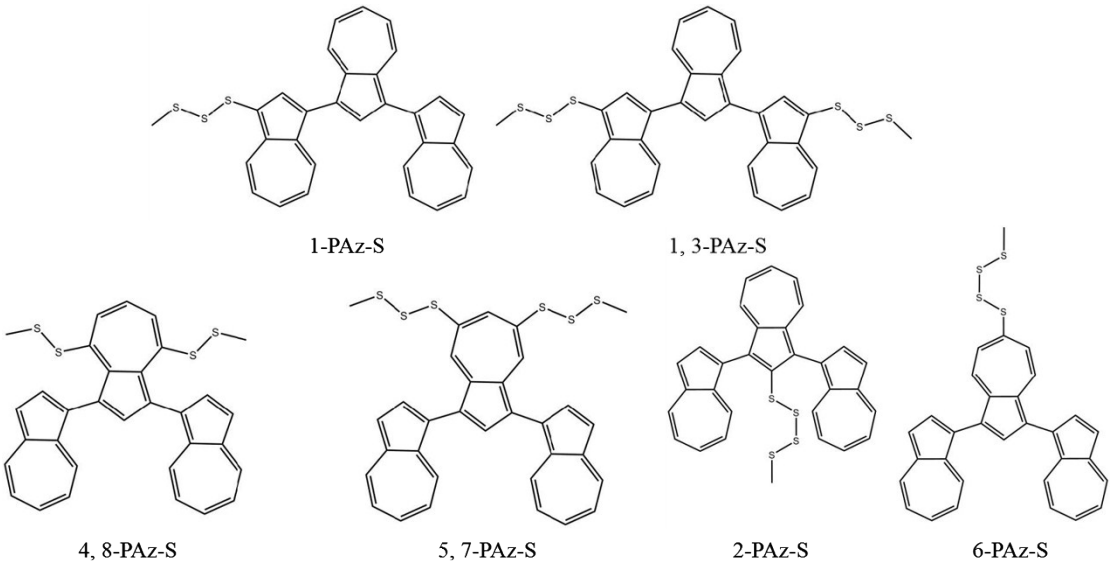

Fig. S9 Chemical structures of PAz-S employed to investigate the influence of the sulfur substitution patterns on the ^{13}C chemical shift.

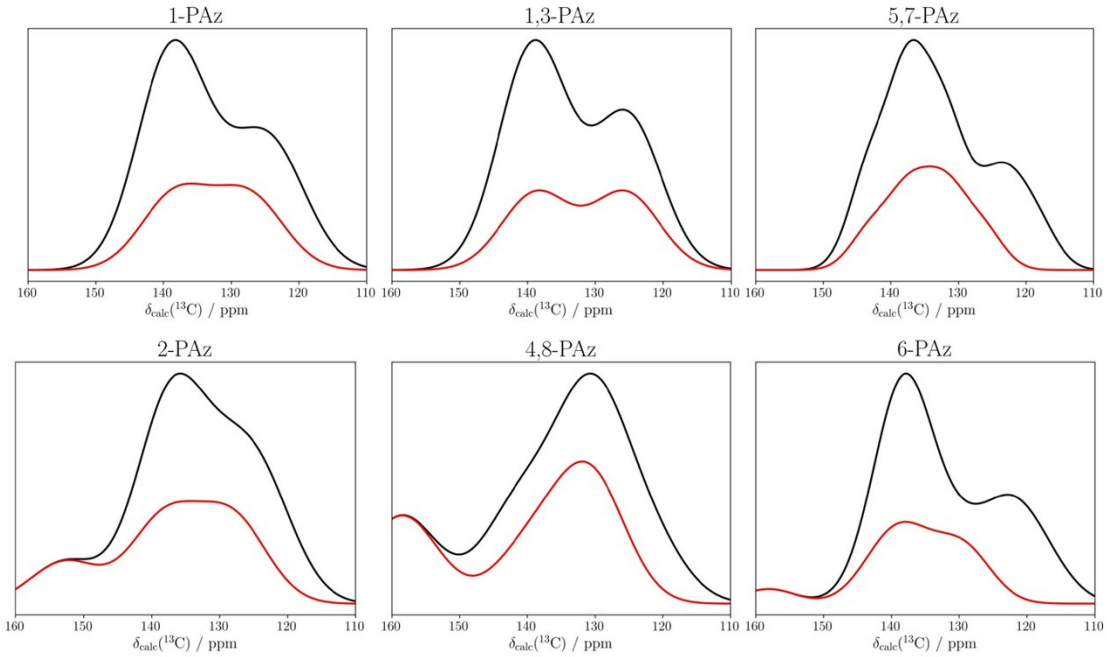

Fig. S10 Plots of the ^{13}C chemical shifts values resulting from DFT calculations of the different sulfur-substitution patterns for PAz-S in Figure S9. Color code: $C_q + CH_x$ (black), C_q (red), CH_x (blue). All calculated ^{13}C shifts are plotted assuming a Gaussian linewidth of 375 Hz to better reflect the broad experimental spectrum in Fig. S8.

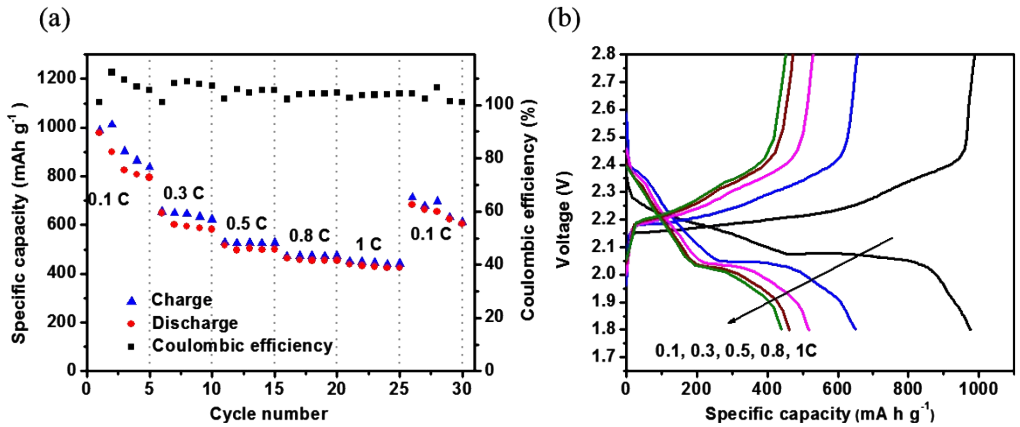

Fig. S11 (a) Rate performance of the Az-S, and (b) charge-discharge profiles at different current density.

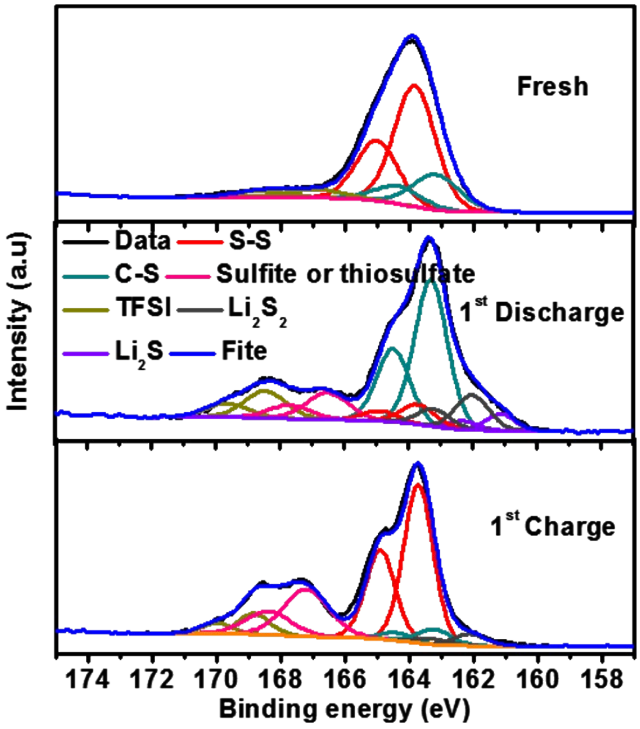

Fig. S12 Ex situ S 2p XPS spectra of pristine Az-S (upper), the Az-S after fully discharging (middle) and the first complete recovery after charging (bottom) at 0.3 C.

In order to get insight to the final discharge and charge product, ex situ XPS was conducted (Fig. S12). The peak located around 168.5 eV corresponds to R=SO_2=R (TFSI anion). The intensity of this peak increases after fully discharging and charging at ~167 eV due to the degradation of the electrolyte. After fully discharging, two low intensity peaks appeared at 162 and 160.9 eV, representing Li_2S_2 and Li_2S, respectively.[9] Furthermore, the intensity of S-S bond decreases sharply, indicating the breaking of S-S bond and the formation of Li_xS. The high intensity of C-S bond indicates the C-S bond is hard to break. After fully charging, reversible formation of S-S bond suggests the stability of organosulfur polymer backbone. However, the peak at 162 eV remains and the ratio of C-S/S-S bonds decreases from 1/2 to

1/5, indicating unsatisfied reversibility during discharge and charge.

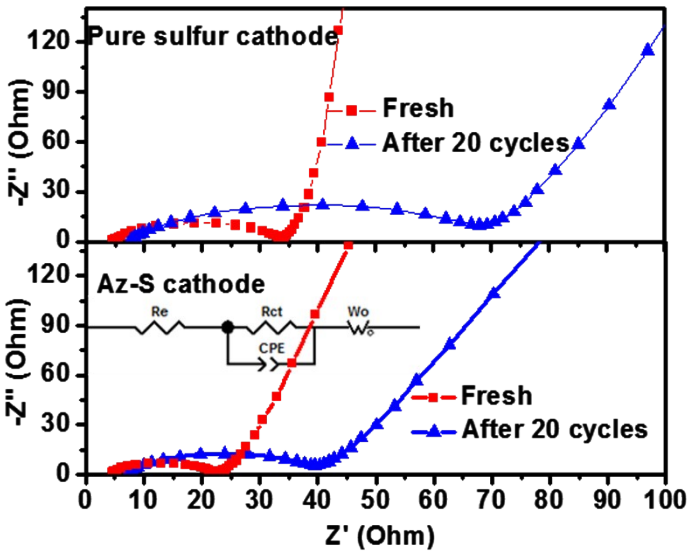

Fig. S13 EIS plots of pure sulfur(upper) and Az-S(lower) as cathode for Li-S batteries at 0.3 C.

Electrochemical impedance spectroscopy (EIS) plots of the cells based on S_8 and Az-S are shown in Fig. S13. The EIS plots compose of depressed semicircles from high to middle frequency and slope lines in the low frequency region. The inset in Fig. S13 displays Randles equivalent circuit model, in which, R_e, R_{ct}, CPE and W_0 are the resistance of electrolyte, charge-transfer resistance, double-layer capacitance, and the Warburg impedance, respectively.[10] Before the discharge and charge cycles, both electrodes show similar low charge transfer resistance. After 20 charging/discharging cycles at 0.3 C, the R_{ct} increases for pure sulfur and Az-S cathodes. It is noted that the R_{ct} for Az-S cathode is much smaller than for the sulfur cathode, indicating a lower passivation on the surface of Az-S and a high charge transfer ability.

Table S1: Elemental analysis of Az-S and PAz-S.

Name	C / wt%	H / wt%	O / wt%	S / wt%
Az-S	29.06	1.69	0.85	68.4
PAz-S	71.29	4.24	13.51	10.96

References:

1. *Organic Syntheses*, 1984, **62**, 134.
2. J. D. Mao and K. Schmidt-Rohr, *Enviro. Sci. Technol.,* 2004, **38**, 2680-2684.
3. R. Ahlrichs, M. Bär, M. Häser, H.Horn, C. Kölmel, *Chem. Phys. Lett.,* 1989, **162**, 165-169.
4. R. Ahlrichs, F. Furchem C. Hättig, TURBOMOLE v6.5 2019, University of Karlsruhe.
5. J. Tao, J.P. Perdew, V.N. Staroverov, G. E. Scuseria, *Phys. Rev. Lett.,* 2003, **91**, 146401.
6. F. Weigend, R. Ahlrichs, *Phys. Chem. Chem. Phys.,* 2005, **7**, 3297-3305.
7. D. Becke, *J. Chem. Phys***.,** 1993, **98**, 5648-5652.
8. P. J. Stephens, F. J. Devlin, C. F. Chabalowski, M. J. Frisch, *Phys. Chem.,* 1994, **98**, 11623-11627.
9. (a) S. H. Je, H. J. Kim, J. Kim, J. W. Choi and A. Coskun, *Adv. Funct. Mater.*, 2017, **27**, 1703947. (b) M. I. Nandasiri, L. E. Camacho-Forero, A. M. Schwarz, V. Shutthanandan, S. Thevuthasan, P. B. Balbuena, K. T. Mueller and V. Murugesan, *Chem. Mater.*, 2017, **29**, 4728-4737.
10. (a) Y. Zhong, X. Xia, S. Deng, J. Zhan, R. Fang, Y. Xia, X. Wang, Q. Zhang and J. Tu, *Adv. Energy Mater.*, 2018, **8**, 1701110; (b) J. Zhou, Y. Guo, C. Liang, L. Cao, H. Pan, J. Yang and J. Wang, *Chem. Commun.*, 2018, **54**, 5478-5481.